HHS Public Access

Author manuscript

Nat Med. Author manuscript; available in PMC 2014 October 01.

Published in final edited form as:

Nat Med. 2014 April ; 20(4): 443–449. doi:10.1038/nm.3495.

Label-free *in vivo* imaging of myelinated axons in health and disease with spectral confocal reflectance microscopy

Aaron J. Schain[1], **Robert A. Hill**[1], and **Jaime Grutzendler**[1,2,*]

[1]Yale University School of Medicine, Department of Neurology, 300 George St. Suite 8201, New Haven, CT 06511

[2]Yale University School of Medicine, Department of Neurobiology, 300 George St. Suite 8201, New Haven, CT 06511

Abstract

We report a new technique for high-resolution *in vivo* imaging of myelinated axons in the brain, spinal cord and peripheral nerve that requires no fluorescent labeling. This method, based on spectral confocal reflectance microscopy (SCoRe), uses a conventional laser scanning confocal system to generate images by merging the simultaneously reflected signals from multiple lasers of different wavelengths. Striking color patterns unique to individual myelinated fibers are generated that facilitate their tracing in dense axonal areas. These patterns highlight nodes of Ranvier and Schmidt-Lanterman incisures and can be used to detect various myelin pathologies. Using SCoRe we performed chronic brain imaging up to 400 μm deep, capturing for the first time *de novo* myelination of mouse cortical axons *in vivo*. We also established the feasibility of imaging myelinated axons in the human cerebral cortex. SCoRe adds a powerful component to the evolving toolbox for imaging myelination in living animals and potentially in humans.

Keywords

Spectral confocal reflectance microscopy; two photon microscopy; myelin; demyelination; in vivo imaging; cortex; spinal cord; sciatic nerve; human brain; multiple sclerosis; oligodendrocyte; neuropathy; node of Ranvier; Schmidt-Lanterman incisures

Introduction

Myelin is a complex cellular structure that plays critical roles in action potential propagation, axonal insulation and trophic support[1] and is a potential site of experience-dependent neural plasticity[2,3]. Oligodendrocytes and Schwann cells, the myelin producing cells, are affected in a variety of pathologies involving the brain, spinal cord and peripheral nerves[4,5].

*Corresponding author: Ph: (203)737-3514, Fax: (203)785-7903, jaime.grutzendler@yale.edu.

Contributions

Project initial design and conception (AJS, JG), experimental design (AJS, RAH, JG), experimental execution (AJS, RAH), data analysis (AJS, RAH, JG), manuscript writing (AJS, RAH, JG), project supervision (JG).

Imaging techniques such as electron and confocal fluorescence microscopy have been invaluable in furthering the cellular understanding of myelin development, plasticity and pathology. Diffusion tensor magnetic resonance imaging (DTI), has allowed longitudinal studies of cerebral white matter tracts in animal models and humans[6], and genetically encoded fluorescent reporters have allowed imaging of oligodendrocytes in living organisms[7,8]. Methods have also been developed for label-free imaging of myelinated fibers using coherent anti-Stokes Raman scattering (CARS)[9–11], optical coherence (OCM) [12] or third harmonic generation (THG)[13,14] microscopy.

We developed a powerful yet easy to implement method for high-resolution label-free *in vivo* imaging of myelinated axons using a conventional laser scanning confocal microscope with tunable wavelength detection capabilities. This method is based on spectral confocal reflectance microscopy (SCoRe) and takes advantage of the high refractive index of lipid-rich myelin[15,16]. Reflection signals are obtained using multiple confocal lasers, which individually generate images of discontinuous segments but when merged, constitute contiguous myelinated axon images.

Using SCoRe we imaged longitudinally for the first time, fine changes in axonal myelination in the living mouse cortex. We were able to track Schmidt-Lanterman incisures and nodes of Ranvier *in vivo* in normal and pathological conditions. We also implemented SCoRe concurrently with confocal fluorescence or two-photon microscopy to image the interactions between axons, oligodendrocytes, and other cell types such as astrocytes and microglia. Finally, we demonstrate in a postmortem human cortical explant that SCoRe can be used for high-resolution imaging of cortical myelinated axons directly through the pial surface.

Results

In vivo imaging of myelinated axons with SCoRe microscopy

We first applied single-wavelength confocal reflectance microscopy through a thinned skull in an anesthetized mouse (Fig. 1). We noticed a reflective network pattern, that although patchy (Fig. 1c), was reminiscent of cortical layer I axons[17]. When using different laser wavelengths, the images remained patchy but did not fully overlap (Fig. 1c). Interestingly, simultaneous imaging with multiple wavelengths gave a complementary reflection pattern that when composited and pseudocolored monochromatically (Fig. 1c–f), appeared as a continuous image, revealing that these processes projected for long distances (Fig. 1b and Supplementary Video 1). Similar wavelengths (476 and 488 nm) tended to generate reflective patches at similar locations along the fiber, while more distant wavelengths (488, 561 and 633 nm) produced less overlapping patches (Fig. 1g–h). Furthermore, the merged images appeared contiguous when using only 488, 561 and 633 nm lasers, and additional wavelengths (Figure 1d–f) or images captured with a white light broadband laser (data not shown), did not lead to more contiguous images. Therefore, we used those lasers for all subsequent experiments.

To better characterize these reflective fibers, we combined *in vivo* SCoRe with confocal fluorescence microscopy. Using mice that express yellow fluorescent protein in a subset of

layer V cortical pyramidal neurons (Thy1-YFP), we found that none of the fluorescent dendrites were reflective, while some reflective processes co-localized with YFP (Fig. 1i and Supplementary Video 1) suggesting that they represented myelinated axons, given myelin's known reflective properties[15,16]. To confirm this, we labeled myelin through a craniotomy with Fluoromyelin (FM) dye and found that it robustly labeled the myelin sheath of superficial cortical axons as evidenced by their tubular appearance (Fig. 2a). We found that 100% of FM-labeled fibers were reflective (Fig. 2a), while YFP-labeled dendrites, unmyelinated axons (FM-negative) (Fig. 2b), astrocytes and microglia (Supplementary Fig. 1) produced no reflectance. Furthermore, FM-negative axonal segments, such as at some axonal bifurcations (Fig. 2c), which lack myelin[18,19], were not reflective, even though the axon was normal as evidenced by intact YFP. Additionally, while imaging peripheral nerves *in vivo* with SCoRe, we found that individual FM-labeled axons lacked reflection at non-myelinated nodes of Ranvier (Figs. 2d, and 4d–f, i–j). These data strongly suggested that myelin is the source of fiber reflection in both cortex and peripheral nerves.

Curiously, even though myelin is the source of reflectance, we observed that when viewed in the XY plane, the signal appeared to arise from the center of the myelinated tube, where the axon is located, rather than from the sides of the tube as seen with FM labeling (Fig. 2). To resolve this apparent contradiction, we analyzed orthogonal (XZ) views of individual axons in the sciatic nerve from Thy1-YFP mice (Supplementary Fig. 2). In the XZ plane, it became apparent that the reflection originates above and below the YFP-labeled axon, generating an hourglass shape, with little reflection observed at the center of the axon (Supplementary Fig. 2a–b, f–g), demonstrating that the source of reflection is indeed the surrounding myelin. This was simulated experimentally by imaging a pulled glass capillary similar in size to an axon, filled with fluorescently-labeled agarose. We found a strikingly similar hourglass reflection shape with the outer and inner glass surfaces being most reflective (Supplementary Fig. 2c–d). This strongly suggests that only the portion of light reflecting at a particular angle of incidence is captured by the confocal detectors (Supplementary Fig. 2e), resulting in the "axonal" appearance in XY projections. Furthermore, measurements of the outer diameter obtained from XZ reflection images, matched almost perfectly those obtained from the XY confocal fluorescent images of FM myelin labeling (Supplementary Figs. 2g, and 3). This not only provides additional confirmation that the reflection signal originates in the myelin sheaths but also constitutes an accurate means for measuring outer fiber diameter *in vivo* in a label-free fashion.

Although, with SCoRe, the wavelengths used are shorter and light collection less efficient than with two-photon microscopy, we were able to detect cortical myelinated axons as deep as 400 μm, even with low laser intensities (~300μW at the sample) (Supplementary Video 2). This is likely explained by the fact that myelin is highly reflective, making light scattering and collection efficiency less critical for SCoRe compared to fluorescence imaging.

Combined use of SCoRe with fluorescence microscopy

To further characterize the reflection signal, we implemented SCoRe simultaneously with fluorescence microscopy in fluorescent reporter-expressing transgenic mice under control of

the proteolipid protein promoter (PLPDsRed)[20]. In these mice, single oligodendrocytes can be visualized in the superficial cortex with either two-photon (Supplementary Fig. 4 a–b) or confocal (Supplementary Fig. 4 c–g) microscopy *in vivo*. However, although their fluorescent processes can be clearly detected, it is not possible to accurately trace individual myelinated axons, because oligodendrocytes have a large number of branches that provide myelin for only a single internode.

Combining SCoRe and confocal fluorescence microscopy *in vivo* allowed us to precisely trace individual myelinated fibers for long distances spanning several internodes. Oligodendrocyte processes were seen running along reflective fibers but several processes especially those close to the oligodendrocyte cell bodies did not produce any reflection, suggesting that they do not form compact myelin sheaths (Supplementary Fig. 4d,g). Thus SCoRe provides unique information about the status of myelin compaction which to our knowledge is not possible with other optical methods. The combination of SCoRe and fluorescence imaging constitutes a powerful tool set for studying oligodendrocyte interactions with axons, formation of a compact myelin sheath, oligodendrocyte injury, myelin degeneration and regeneration.

Distinct patterns of cortical myelin dynamics in neonates and adults

We used SCoRe for time-lapse imaging of layers I–II cortical myelin in mice of various ages. Consistent with the known time course of cortical myelin development[22], mice younger than 2 weeks, had neither reflective nor FM stained axons (data not shown) but around P18–21, reflective fibers that appeared as patches (~200 μm in diameter), were first detected (Fig 3 and Supplementary Fig. 5), closely resembling the morphology of individual myelinating oligodendrocytes[23] (Supplementary Fig. 5). At subsequent developmental stages and into adulthood we found a steady increase in the density of reflective axons (Fig. 3a).

Repeated imaging of the same regions over weeks revealed cortical sub-regions that became myelinated, likely due to the maturation of individual oligodendrocytes (Fig. 3b) and also individual axons which became newly myelinated (Fig. 3c–e), stable unmyelinated regions consistent with nodes of Ranvier (Fig. 3f), and unchanged myelinated regions in older animals (Fig. 3g–h). These examples show how fine myelin dynamics can be investigated during development and in the adult using SCoRe.

The spectral reflectance highlights unique myelin features

The reflectance signal from various lasers not only produced a contiguous myelinated axonal image (Fig. 1c–f), but at high zoom appeared as a spectral speckled pattern (Fig. 1c). Remarkably, despite this heterogeneous speckle, in the spinal cord and sciatic nerve, individual axons also had a predominant reflectance color that allowed us to distinguish them from adjacent axons (Fig. 4 and Supplementary Video 3) and could be used for identification of axons over time as the pattern changed minimally over days and was not significantly affected by axial sample rotations (Supplementary Fig. 6). The reflection signal is likely to originate from changes in refractive index between the mostly aqueous neural tissue[24] and the lipid-rich myelin, while the multicolor reflection is likely due to thin-film

interference[25], which leads to constructive and destructive interference of particular wavelengths, depending on differences in the thickness of the reflective surface (See Supplementary Fig. 2). Therefore, the number, thickness, and relative composition of the membranous myelin layers may have a direct impact on the reflected spectrum. The most likely explanation for the differences in the overall color of adjacent axons in the peripheral nerve and spinal cord is the large inter-axonal variability in diameter and degree of myelination in contrast with the more homogeneous axons in the superficial cortex. Regardless of the precise mechanism, these colors allow the identification and tracing of individual axons over long distances in peripheral nerves and spinal cord (Fig. 4).

High-resolution imaging in the sciatic nerve revealed a peculiar periodic vertical multicolor reflection pattern at irregular intervals of approximately 20–60μm (Fig. 4d–j). To investigate its cellular origin, we reasoned that mT/mG transgenic mice, which express tdTomato in cell membranes, would be useful for simultaneously imaging myelin and its reflection in peripheral nerves. Indeed, we observed highly detailed images of myelin layers (Supplementary Fig. 3) and noticed the typical oblique appearance of Schmidt-Lanterman incisures (SLI)[26] (Fig. 4d). Remarkably, these periodic vertical reflection areas completely colocalized with fluorescent SLIs. These incisures are cytoplasmic channels, within the otherwise compact myelin that are critical for molecular flow along myelin layers[26]. To our knowledge, SCoRe is the only label-free technique that can unambiguously image these structures *in vivo*, opening the possibility of studying them in the context of a variety of pathologies.

Imaging myelin pathology and the human brain with SCoRe

To determine if SCoRe is able to detect myelin defects, we used *shiverer* mice, a well-known model in which mutation of the myelin basic protein (MBP) gene prevents the formation of compact myelin in the CNS. *In vivo* imaging of the cortex of *shiverer* mice showed a marked paucity of reflective fibers (Fig. 5), with occasional small scattered segments of reflectance but no continuous axons (Fig. 5d). To test if these were areas lacking myelin, we labeled the cortex by topical application of Fluoromyelin (FM). Indeed, *shiverer* mice had severely reduced labeling, but the small scattered areas of reflection uniformly colocalized with FM labeling (Fig. 5d). Imaging on brain slices from *shiverer* mice confirmed the dramatic reduction in the reflection signal in the corpus callosum (Supplementary Fig. 7). This demonstrates unambiguously that the reflectance signal is dependent on the presence of compact myelin and shows that SCoRe is a sensitive method for detecting central myelination defects.

We also imaged the sciatic nerve of *shiverer* mice as these have been reported to have alterations in the number of Schmidt-Lanterman incisures[27]. Indeed, we were able to show that these mice have increased density of SLIs (Supplementary Fig. 7), demonstrating that SCoRe is able to detect *in vivo* very subtle peripheral myelin changes. In addition, we were able to demonstrate rapid changes in the multicolor pattern after exposure to the demyelinating agent lysophosphatidylcholine (LPC), Dimethyl sulfoxide (DMSO) or a hypotonic solution (Fig. 5 e–f and Supplementary Fig. 8) and also detected changes in myelination during axonal degeneration and regeneration after sciatic nerve crush

(Supplementary Fig. 8). Thus, SCoRe can be used to detect a variety of myelin pathologies *in vivo.*

Finally, we imaged a paraformaldehyde fixed postmortem human brain explant to determine if myelinated fibers could be detected in the human cortex. We oriented the tissue to image the surface of the cortex mimicking the situation for *in vivo* imaging of mouse brain (Fig. 5g). Consistent with mouse images, we saw a highly reflective network of axons (Fig. 5h) that colocalized with Fluoromyelin labeling (Fig. 5i), confirming these were indeed myelinated axons. These data show the feasibility of imaging myelinated axons in human tissue with high resolution, low laser power and no dye administration.

Discussion

In vivo optical imaging has been invaluable for understanding the plasticity of cells in the nervous system during development, aging and pathology[28–30]. We have developed a technique that allows label-free high-resolution *in vivo* imaging of myelinated axons using spectral confocal reflectance microscopy (SCoRe). Because SCoRe only requires a confocal microscope with tunable wavelength detection capabilities, which is routinely used throughout the world, this technique could have wide applications in preclinical animal studies of myelin pathologies. In addition, SCoRe has the potential to be adapted as a tool for *in vivo* human peripheral and cortical myelin imaging.

Although the precise mechanism for the multicolor reflection is not clear, it likely relates to the principle of thin-film interference[25]. Similar to dichroic mirrors with alternating layers of optical coatings of different refractive indices, myelin is composed of many layers of lipid-rich sheaths. This layered structure leads to constructive and destructive light interference, reinforcing certain reflected wavelengths and suppressing others (Supplementary Fig. 2). The thickness and number of layers may determine the wavelengths that are preferentially reflected, with further variability due to focal irregularities in myelin sheath thickness, lipid composition and other local cellular variables. Interestingly, we found that in addition to the focal color patchiness, individual axons displayed a unique overall color signature. These unique color features of individual axons in the spinal cord and peripheral nerve facilitated their identification and tracing during time-lapse imaging despite the high density of adjacent processes (Figs. 4 and Supplementary Fig. 6), analogous to methods like Brainbow[32] or Diolistic labeling[33]. We also found in peripheral nerve axons a striking periodic multicolor reflection pattern derived from Schmidt-Lanterman incisures; which can now be studied *in vivo*.

Several methods are currently available for *in vivo* imaging of myelin and myelin producing cells. Confocal and two photon microscopy has been used with genetically encoded fluorescent markers in zebra fish oligodendrocytes[7]. Using these fluorescent reporters, however, it is not easy to trace individual myelinated axons or determine when oligodendrocyte cellular processes near an axon have established a mature compact myelin sheath. Furthermore, although fluorescent dyes such as Fluoromyelin can be useful for *in vivo* imaging, labeling with these dyes is not consistent, making them unsuitable for longitudinal imaging. SCoRe, however, provides a uniform traceable image of the axon, is

very sensitive to the presence of a compact myelin sheath and allows repeated transcranial imaging of fine structural myelin changes (Supplementary Fig. 6 and Fig. 3).

While label-free methods such as OCM, CARS and THG have great potential, they require complex setups or rarely available equipment, whereas SCoRe uses a conventional confocal microscope making it easy to implement. Furthermore, because SCoRe is highly sensitive to myelin, it requires light levels that are substantially lower (on the order of 200–400 μW at the sample) than those used for conventional confocal fluorescence or two photon microscopy. Thus, this technique can be used for repeated imaging at high zooms with virtually no photo-toxicity or thermal injury (Fig. 3), making it ideal for *in vivo* use. Longer wavelength Ti:sapphire lasers, can also be used (data not shown), which would in theory allow it to achieve greater penetration than two photon microscopy as both incident and reflected lights would be infrared and thus less scattering.

Using SCoRe, we made several novel observations *in vivo*: we tracked longitudinally for the first time newly formed myelinated structures in the living mammalian brain and found that myelination progresses rapidly over days (Fig. 3) but change is confined to isolated micro-regions (Fig. 3 and Supplementary Fig. 5), likely representing territories of single oligodendrocytes. Second, we found areas lacking myelination at axonal bifurcations in the cortex, an under-investigated phenomenon[18] that can now be studied *in vivo*. Third, we imaged for the first time longitudinally in a mouse, Schmidt-Lanterman incisures (Fig. 4) and nodes of Ranvier (Figs. 3 and 4). Fourth, by concurrently using SCoRe with fluorescence imaging, we showed that a substantial number of proximal oligodendrocyte processes do not form a compact myelin sheath.

Future modifications of SCoRe with infrared laser excitation and detection capabilities[36] or fiber-optic coupling, would increase the imaging depth, and may eventually allow imaging of human brain, spinal cord and peripheral nerve. For example, recently it has become possible to generate myelin with engrafted neural stem cells in humans with severe leukodystrophies[35,37]. Additionally, it has been documented that subpial cortical demyelination is one of the earliest pathological events in multiple sclerosis[38,39]. SCoRe, which allows high resolution imaging in the intact cortex, could potentially be used for tracking the formation of myelin after engraftment or its degeneration in severe demyelinating disorders or traumatic brain injury. An approach based on SCoRe could also be applied for imaging peripheral nerves instead of tissue biopsy in various polyneuropathies. Thus, SCoRe is a powerful technique that adds significant capabilities to the toolbox for *in vivo* imaging of the central and peripheral nervous systems in animal models and potentially in humans.

Online Methods

Animals

All animal procedures were approved by and carried out in accordance with Yale University IACUC guidelines and were performed on both male and female mice aged P15–P480 as indicated in the text. Mouse lines used included Thy1-YFP line H[40] (Jackson Labs # 003782), CX3CR1-GFP[41] (Jackson Labs #005582), MBP^{shi} (Jackson Labs #001428),

mT/mG[42] (Jackson Labs #007576) and C57BL/6 (Jackson Labs #000664), PLPDsRed[20]. Postmortem human tissue was a deidentified tissue sample from a deceased individual from the Northwestern Alzheimer Disease Center IRB-approved Tissue Bank. No investigator blinding for group allocation was necessary for the experiments described in this study. No statistical methods were used to predetermine sample size. Randomization and a power analysis were not necessary for this study.

Spectral Confocal Reflectance Microscopy

We used a Leica SP5 confocal microscope with a water immersion objective (Leica 20x, 1.0 NA), using 458, 476, 488, 514, 561, and 633 nm laser wavelength outputs sent through an Acousto-Optical Tunable Filter (AOTF) and a 30/70 partially reflective mirror. The reflected light was collected using three photodetectors set to collect light through narrow bands defined by prism and mirror-sliders, centered around the laser wavelengths, 486–491nm, 559–564nm, and 631–636nm respectively. The channels from each photodetector were then considered independently, additively combined into one channel, or shown as a color composite with 488 as blue, 561 as green, and 633 as red. For detailed spectral analysis we also used a broadband white light laser (Leica SP8 confocal microscope, with a multi-immersion objective 20x, 0.75 NA). Laser intensities for SCoRe ranged from 200–400 μW at the sample depending on the preparation used (thin skull vs. cranial window), the tissue being imaged, and the specific laser as longer wavelength lasers required less power for sufficient signal and penetration. Images were analyzed using NIH ImageJ. 3D reconstructions were created with Imaris imaging software (Bitplane Scientific Software).

Two-photon Imaging

We used a mode locked MaiTai tunable laser (Spectra Physics) with a two photon microscope (Prairie Technologies) tuned to 1040nm for imaging of DsRed. Images were taken with a water immersion objective (Leica 20x, 1.0 NA) at depths up to 300 μm below the pial surface.

In vivo imaging of the mouse cortex

The thin skull procedure was used for acute and chronic trans-cranial imaging as described previously[17] while the cranial window procedure was used for acute imaging sessions with dye labeling. Briefly, mice were fully anesthetized using isoflurane (MBP *shiverer*) or Ketamine/Xylazine, and the scalp was shaved and sterilized. A midline scalp incision was made, and a custom made metal plate was affixed to the skull using cyanoacrylate. An area no more than 1mm was thinned with a high speed drill and a microsurgical blade to a thickness of 20–30 μm, or removed along with the underlying dura for the cranial window. For fluorescent myelin labeling, Fluoromyelin (Life Technologies) was applied directly to the exposed cortex in a 50% dilution in PBS from stock solution for 45 minutes and then washed thoroughly. Occasionally, we observed reflective fibers that were partially labeled with Fluoromyelin which was likely due to regional variation in dye penetration resulting in incomplete dye labeling. Cortical vasculature was visualized with intravenous injection of 70,000 MW Texas red dextran (Life Technologies). For astrocyte labeling 50 μM sulforhodamine 101[43] dissolved in PBS was applied for 20 minutes to the exposed cortex

and then washed thoroughly. A #0 glass coverslip cut to size was placed over the cranial window and glued in place using cyanoacrylate.

In vivo imaging of the sciatic nerve

Mice were fully anesthetized using Ketamine/Xylazine and the skin was thoroughly shaved and sterilized on the lower back and upper thigh. A small incision was made in the skin above the plane between the vastus lateralis and the biceps femoris muscles. The skin was gently dissected from the underlying musculature and the sciatic nerve was exposed by separating the vastus lateralis and biceps femoris and separated from the surrounding connective tissue. A custom made metal rod was used to gently elevate the separated nerve to immobilize it for imaging. After imaging, the nerve was lowered back into its original location and the incision was sutured. In some cases, fine #5 forceps were used to cause a controlled crush injury of the nerve. The nerve was pinched for 20 seconds to cause a reproducible crush without severing the nerve. The nerve was imaged before, immediately after, and at one subsequent time point (5–10 days). Otherwise, for acute myelin damage, 1 μL of 2.5% lysophosphatidylcholine (LPC, Sigma Aldrich), 100% DMSO, or 100% double distilled water was injected into the sciatic nerve with a small pulled glass micropipette. Additionally, myelin within the sciatic nerve was sometimes labeled with a direct injection of 0.5–2 μL of Fluoromyelin using a glass electrode This was necessary because the dyes would not diffuse across the surrounding epineurium.

In some cases when projecting images for figure display (Figure 4g and j), it was necessary to merge single 1 μm z-sections that were 3 μm apart, because the best alternating interference pattern signal comes from the top of the axon while the ideal fluorescence incisure signal comes from the middle of the axon.

In vivo imaging of the spinal cord

Mice were fully anesthetized using Ketamine/Xylazine and the back of the mouse was shaved and sterilized with alcohol and betadine. A dorsal midline incision of ~1.5cm was made over vertebrae T10 to L2 and the muscles surrounding the spinous and transverse processes were gently removed to expose the underlying vertebrae. Two standard sterilized staples were used as small anchors and were glued with surgical grade cyanoacrylate to the pedicles of the vertebrae then further secured with dental cement[44]. A small custom shaped metal rod was placed in the dental cement to serve as an anchor point to immobilize the animal during imaging sessions. Next, a laminectomy was performed on 1 vertebra using a small set of dissecting scissors. 1% low melting agarose was applied to the exposed spinal cord and then a #0 glass coverslip was secured on top of the agarose with cyanoacrylate and then dental cement. After the dental cement had dried the animal was secured to a custom built holder for imaging. In some cases 1 μL of Fluoromyelin dye was injected into the spinal cord to label myelin.

Human explant imaging

A 4% paraformaldehyde fixed explant of human brain (entorhinal cortex) was oriented to perform SCoRe imaging through the pial surface as shown in Figure 5g. Laser intensities necessary for optimal SCoRe signal were similar to those used for *in vivo* mouse imaging

(200–400 μW at the sample) with a 20x 1.0 NA water immersion objective. Fluoromyelin was applied to the cortical surface for 20 minutes to label myelin within the superficial cortex and then washed thoroughly with PBS.

Glass micropipette imaging

Pulled glass micropipettes (diameters ranging from 2–20μm) were filled with 1% agarose containing Alexa 488 dye and then immersed in PBS for imaging. Pipettes were imaged with SCoRe and fluorescence with identical settings to those used for in vivo SCoRe imaging of both the cortex and sciatic nerve.

Supplementary Material

Refer to Web version on PubMed Central for supplementary material.

Acknowledgments

This study was supported by the following Grants: R01AG027855 and R01HL106815 (JG). We would like to thank J. Bewersdorf and D. Toomre for helpful discussions and P. Yuan for critical reading of the manuscript. We thank A. Nishiyama (University of Connecticut, Storrs CT USA) and F. Kirchhoff (University of Saarland, Homburg Germany) for providing PLPDsRed mice. Postmortem human specimen was obtained from the brain bank in the Cognitive Neurology and Alzheimer's disease Center (CNADC) at Northwestern University (Grant #AG13854).

References

1. Nave KA. Myelination and support of axonal integrity by glia. Nature. 2010; 468:244–52. [PubMed: 21068833]
2. Zatorre RJ, Fields RD, Johansen-Berg H. Plasticity in gray and white: neuroimaging changes in brain structure during learning. Nat Neurosci. 2012; 15:528–36. [PubMed: 22426254]
3. Liu J, et al. Impaired adult myelination in the prefrontal cortex of socially isolated mice. Nat Neurosci. 2012; 15:1621–3. [PubMed: 23143512]
4. Franklin RJM, Ffrench-Constant C. Remyelination in the CNS: from biology to therapy. Nat Rev Neurosci. 2008; 9:839–55. [PubMed: 18931697]
5. Fancy SPJ, Chan JR, Baranzini SE, Franklin RJM, Rowitch DH. Myelin regeneration: a recapitulation of development? Annu Rev Neurosci. 2011; 34:21–43. [PubMed: 21692657]
6. Bartzokis G, et al. Multimodal magnetic resonance imaging assessment of white matter aging trajectories over the lifespan of healthy individuals. Biol Psychiatry. 2012; 72:1026–34. [PubMed: 23017471]
7. Kirby BB, et al. In vivo time-lapse imaging shows dynamic oligodendrocyte progenitor behavior during zebrafish development. Nat Neurosci. 2006; 9:1506–11. [PubMed: 17099706]
8. Kaya F, et al. Live imaging of targeted cell ablation in Xenopus: a new model to study demyelination and repair. J Neurosci. 2012; 32:12885–95. [PubMed: 22973012]
9. Wang H, Fu Y, Zickmund P, Shi R, Cheng JX. Coherent anti-stokes Raman scattering imaging of axonal myelin in live spinal tissues. Biophys J. 2005; 89:581–91. [PubMed: 15834003]
10. Fu Y, Huff TB, Wang HW, Wang H, Cheng JX. Ex vivo and in vivo imaging of myelin fibers in mouse brain by coherent anti-Stokes Raman scattering microscopy. Opt Express. 2008; 16:19396–409. [PubMed: 19030027]
11. Imitola J, et al. Multimodal coherent anti-Stokes Raman scattering microscopy reveals microglia-associated myelin and axonal dysfunction in multiple sclerosis-like lesions in mice. J Biomed Opt. 2011; 16:021109. [PubMed: 21361672]
12. Ben Arous J, et al. Single myelin fiber imaging in living rodents without labeling by deep optical coherence microscopy. J Biomed Opt. 2011; 16:116012. [PubMed: 22112117]

13. Witte S, et al. Label-free live brain imaging and targeted patching with third-harmonic generation microscopy. Proc Natl Acad Sci USA. 2011; 108:5970–5. [PubMed: 21444784]
14. Farrar MJ, Wise FW, Fetcho JR, Schaffer CB. In vivo imaging of myelin in the vertebrate central nervous system using third harmonic generation microscopy. Biophys J. 2011; 100:1362–71. [PubMed: 21354410]
15. Filler TJ, Peuker ET. Reflection contrast microscopy (RCM): a forgotten technique? J Pathol. 2000; 190:635–8. [PubMed: 10727991]
16. Xiao J, Levitt JB, Buffenstein R. The use of a novel and simple method of revealing neural fibers to show the regression of the lateral geniculate nucleus in the naked mole-rat (Heterocephalus glaber). Brain Res. 2006; 1077:81–9. [PubMed: 16483554]
17. Grutzendler J, Kasthuri N, Gan WB. Long-term dendritic spine stability in the adult cortex. Nature. 2002; 420:812–6. [PubMed: 12490949]
18. Waxman SG. Ultrastructural observations on branching patterns of central axons. Neurosci Lett. 1975; 1:251–6. [PubMed: 19604786]
19. Ha H. Axonal bifurcation in the dorsal root ganglion of the cat: a light and electron microscopic study. J Comp Neurol. 1970; 140:227–40. [PubMed: 4097270]
20. Hirrlinger PG, et al. Expression of reef coral fluorescent proteins in the central nervous system of transgenic mice. Mol Cell Neurosci. 2005; 30:291–303. [PubMed: 16169246]
21. Yang G, Pan F, Parkhurst CN, Grutzendler J, Gan WB. Thinned-skull cranial window technique for long-term imaging of the cortex in live mice. Nat Protoc. 2010; 5:201–8. [PubMed: 20134419]
22. Jacobson S. Sequence of myelination in the brain of the albino rat. A Cerebral cortex, thalamus and related structures. J Comp Neurol. 1963; 121:5–29. [PubMed: 14051846]
23. Chong SYC, et al. Neurite outgrowth inhibitor Nogo-A establishes spatial segregation and extent of oligodendrocyte myelination. Proc Natl Acad Sci USA. 2012; 109:1299–304. [PubMed: 22160722]
24. Binding J, et al. Brain refractive index measured in vivo with high-NA defocus-corrected full-field OCT and consequences for two-photon microscopy. Opt Express. 2011; 19:4833–47. [PubMed: 21445119]
25. Macleod, HA. Thin-Film Optical Filters Sciences New York. Vol. 668. Institute of Physics Publishing; 2001.
26. Balice-Gordon RJ, Bone LJ, Scherer SS. Functional gap junctions in the schwann cell myelin sheath. J Cell Biol. 1998; 142:1095–104. [PubMed: 9722620]
27. Gould RM, Byrd AL, Barbarese E. The number of Schmidt-Lanterman incisures is more than doubled in shiverer PNS myelin sheaths. J Neurocytol. 1995; 24:85–98. [PubMed: 7745445]
28. Lam CK, Yoo T, Hiner B, Liu Z, Grutzendler J. Embolus extravasation is an alternative mechanism for cerebral microvascular recanalization. Nature. 2010; 465:478–82. [PubMed: 20505729]
29. Davalos D, et al. ATP mediates rapid microglial response to local brain injury in vivo. Nat Neurosci. 2005; 8:752–8. [PubMed: 15895084]
30. Harb R, Whiteus C, Freitas C, Grutzendler J. In vivo imaging of cerebral microvascular plasticity from birth to death. J Cereb Blood Flow Metab. 2012
31. Poliak S, Peles E. The local differentiation of myelinated axons at nodes of Ranvier. Nat Rev Neurosci. 2003; 4:968–80. [PubMed: 14682359]
32. Livet J, et al. Transgenic strategies for combinatorial expression of fluorescent proteins in the nervous system. Nature. 2007; 450:56–62. [PubMed: 17972876]
33. Gan WB, Grutzendler J, Wong WT, Wong RO, Lichtman JW. Multicolor “DiOlistic” labeling of the nervous system using lipophilic dye combinations. Neuron. 2000; 27:219–25. [PubMed: 10985343]
34. Kirschner, Da; Caspar, DL. Myelin structure transformed by dimethylsulfoxide. Proc Natl Acad Sci USA. 1975; 72:3513–7. [PubMed: 1059139]
35. Gupta N, et al. Neural stem cell engraftment and myelination in the human brain. Sci Transl Med. 2012; 4:155ra137.

36. Hong G, et al. Multifunctional in vivo vascular imaging using near-infrared II fluorescence. Nature Medicine. 2012; 18:1841–1846.
37. Windrem MS, et al. Neonatal chimerization with human glial progenitor cells can both remyelinate and rescue the otherwise lethally hypomyelinated shiverer mouse. Cell Stem Cell. 2008; 2:553–65. [PubMed: 18522848]
38. Bø L, Vedeler CA, Nyland HI, Trapp BD, Mørk SJ. Subpial demyelination in the cerebral cortex of multiple sclerosis patients. J Neuropathol Exp Neurol. 2003; 62:723–32. [PubMed: 12901699]
39. Lucchinetti CF, et al. Inflammatory cortical demyelination in early multiple sclerosis. N Engl J Med. 2011; 365:2188–97. [PubMed: 22150037]
40. Feng G, et al. Imaging neuronal subsets in transgenic mice expressing multiple spectral variants of GFP. Neuron. 2000; 28:41–51. [PubMed: 11086982]
41. Jung S, et al. Analysis of fractalkine receptor CX(3)CR1 function by targeted deletion and green fluorescent protein reporter gene insertion. Mol Cell Biol. 2000; 20:4106–4114. [PubMed: 10805752]
42. Muzumdar MD, Tasic B, Miyamichi K, Li L, Luo L. A global double-fluorescent Cre reporter mouse. Genesis. 2007; 45:593–605. [PubMed: 17868096]
43. Nimmerjahn A, Kirchhoff F, Kerr JND, Helmchen F. Sulforhodamine 101 as a specific marker of astroglia in the neocortex in vivo. Nat methods. 2004; 1:31–7. [PubMed: 15782150]
44. Fenrich KK, et al. Long-term in vivo imaging of normal and pathological mouse spinal cord with subcellular resolution using implanted glass windows. J physiol. 2012; 590:3665–75. [PubMed: 22641787]

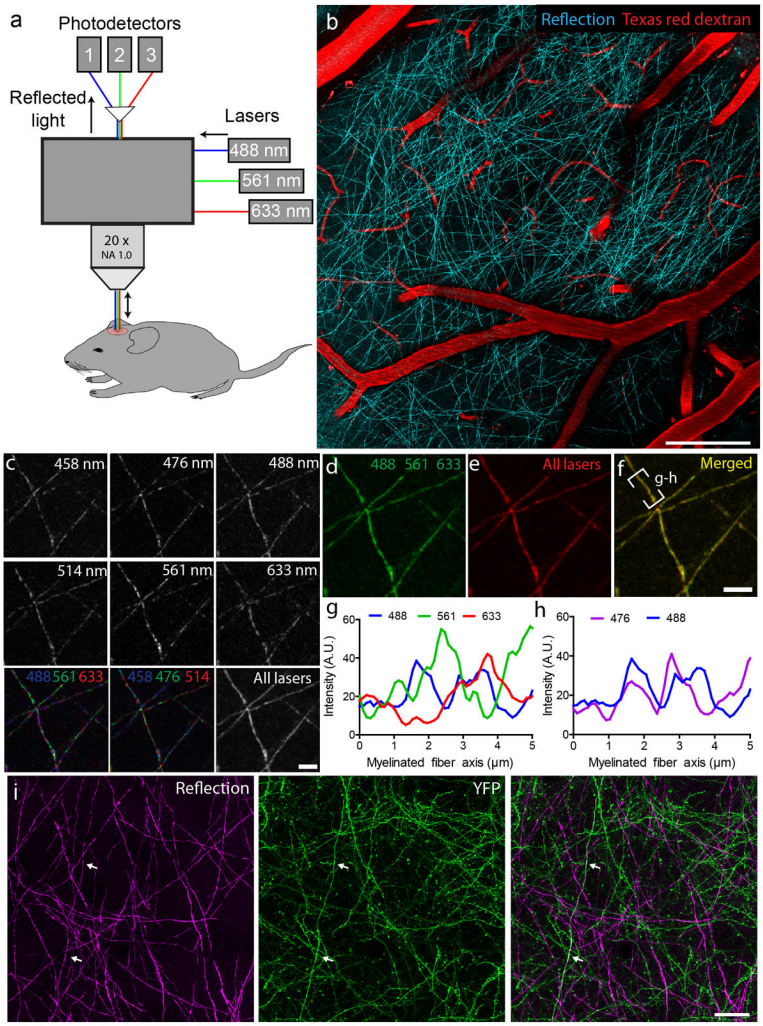

Figure 1. ***In vivo*** **imaging of mouse cortex using spectral confocal reflectance microscopy (SCoRe)**

(**a**) Diagram depicting the imaging and optical setup of SCoRe. Three laser wavelengths are emitted simultaneously and reflect off structures in the mouse cortex. Out of focus light is rejected by the pinhole within the microscope, and the reflected light is separated by a prism into three separate photodetectors. (**b**) Simultaneous imaging of brain vasculature with intravenous injection of fluorescent dextran (red) and combined-wavelength image of reflective fibers (cyan) in the somatosensory cortex. Z-projection over 15 μm. 100 μm scale bar. (**c**) High magnification images of monochromatic reflective signal captured with the 458, 476 488, 514, 561, and 633 nm lasers and then merged as indicated (bottom panels). 5 μm scale bar. (**d–f**) Comparison of all lasers to 488, 561 and 633 shows that these three are sufficient for full fiber detection. 5 μm scale bar. (**g**) Graph showing the reflection intensity along the axon boxed in **f** demonstrating that lasers of wavelengths 488, 561 and 633 nm have some overlapping but mostly non-overlapping reflection peaks. (**h**) Graph showing the reflection pattern of similar wavelengths (476 and 488 nm) is mostly overlapping. (**i**) SCoRe Z-projection (magenta) captured from a Thy1-YFP mouse showing a YFP-labeled axon

(green) that is reflective (arrows), however most YFP-labeled axons and all dendrites are not reflective. 50 μm scale bar (experiments were replicated 3 times in n=15 mice).

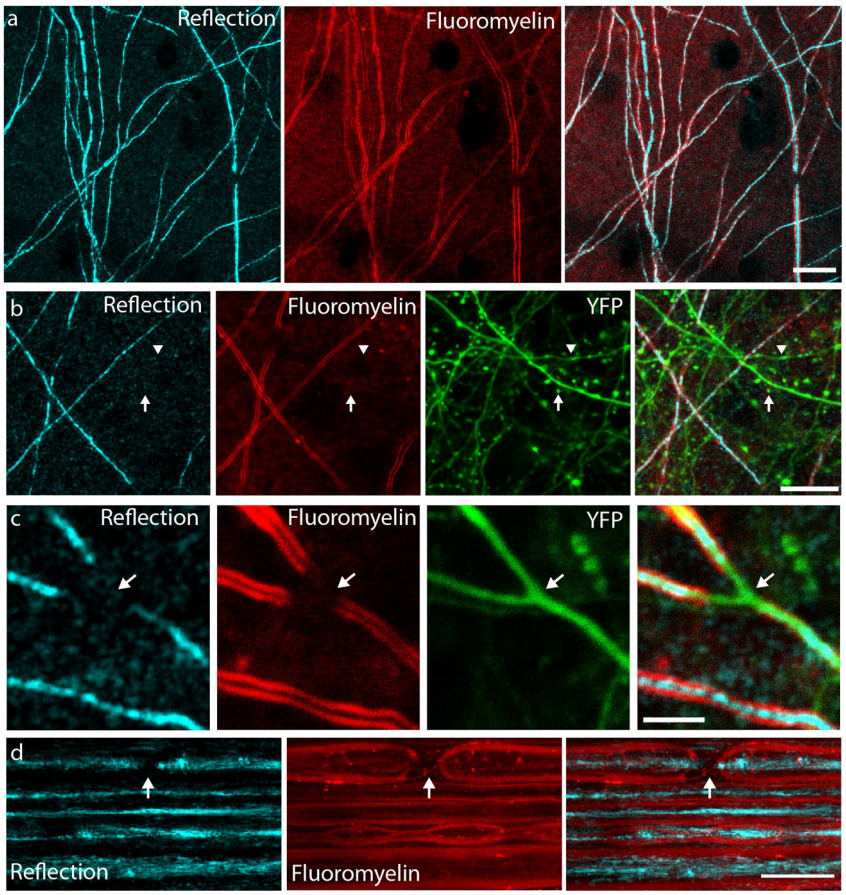

Figure 2. SCoRe signal is dependent on myelination

(**a**) *In vivo* staining of cortical myelin with Fluoromyelin (FM) (red) labels only the reflective fibers (cyan). 10 μm scale bar. (**b**) *In vivo* FM staining in the cortex of a Thy1-YFP mouse showing that YFP-labeled axons (green), that are FM negative and therefore unmyelinated axons (arrowhead), are not reflective. Dendrites (arrow), which are never myelinated, are also not reflective. However, all FM positive segments are reflective (cyan). 10 μm scale bar. (**c**) Example of an axonal bifurcation in a Thy1-YFP mouse imaged *in vivo* demonstrating that specific parts of an axon that are FM positive are also reflective, however the unmyelinated, FM negative portions of the same axon are not reflective (arrow). 3 μm scale bar. (**d**) *In vivo* staining and imaging of myelin in the sciatic nerve with FM (red), reveals the location of nodes of Ranvier (arrows) which lack reflection (cyan). 15 μm scale bar (experiments were replicated 3 times in n=13 mice).

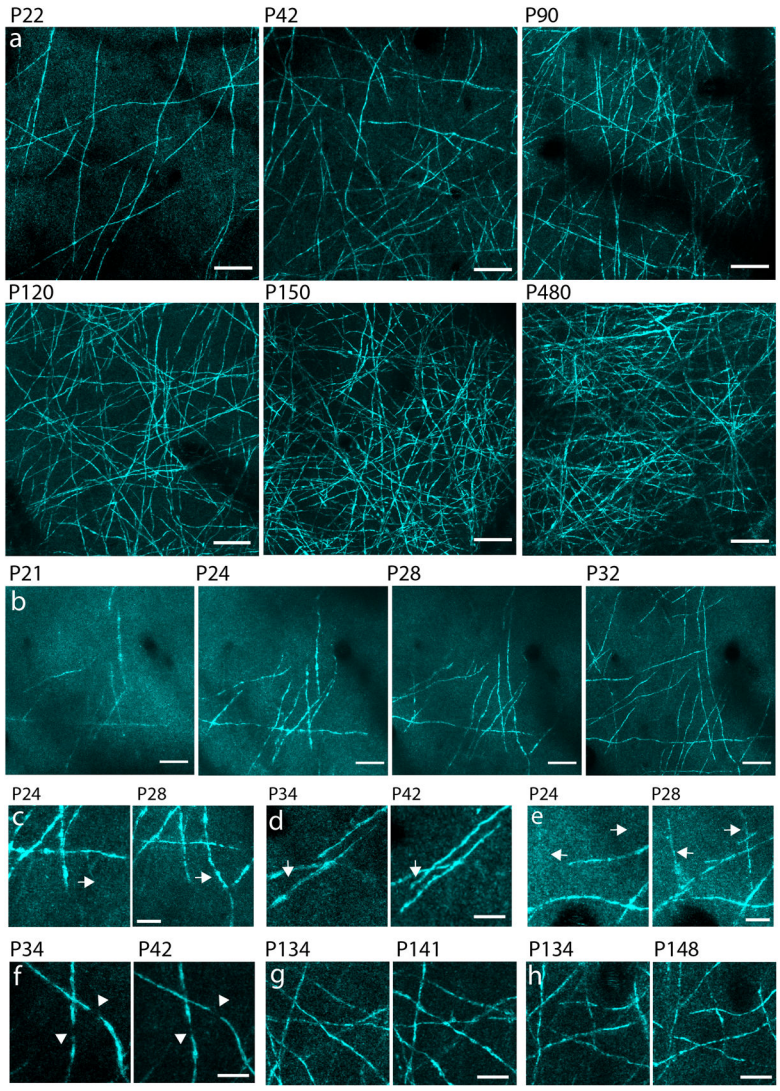

Figure 3. Transcranial time-lapse imaging of the mouse cortex reveals progressive age-dependent myelination

(**a**) *In vivo* SCoRe z-projections taken from the mouse somatosensory cortex at various postnatal ages. (**b**) Images of the same cortical region captured through a thinned skull over four time points showing the appearance of new reflecting fibers. 20 μm scale bars in a–b. (**c–e**) High magnification z-projections of specific axons that were myelinated between imaging sessions (arrows) at the ages indicated, demonstrating that SCoRe reveals new myelin formation *in vivo*. (**f–h**) Z-projections showing repeated imaging of suspected nodes of Ranvier (**f**) (arrowheads) and stable myelinated axons (**g–h**) in older animals. 10 μm scale bars in c–h (experiments were replicated 3 times in n=9 mice).

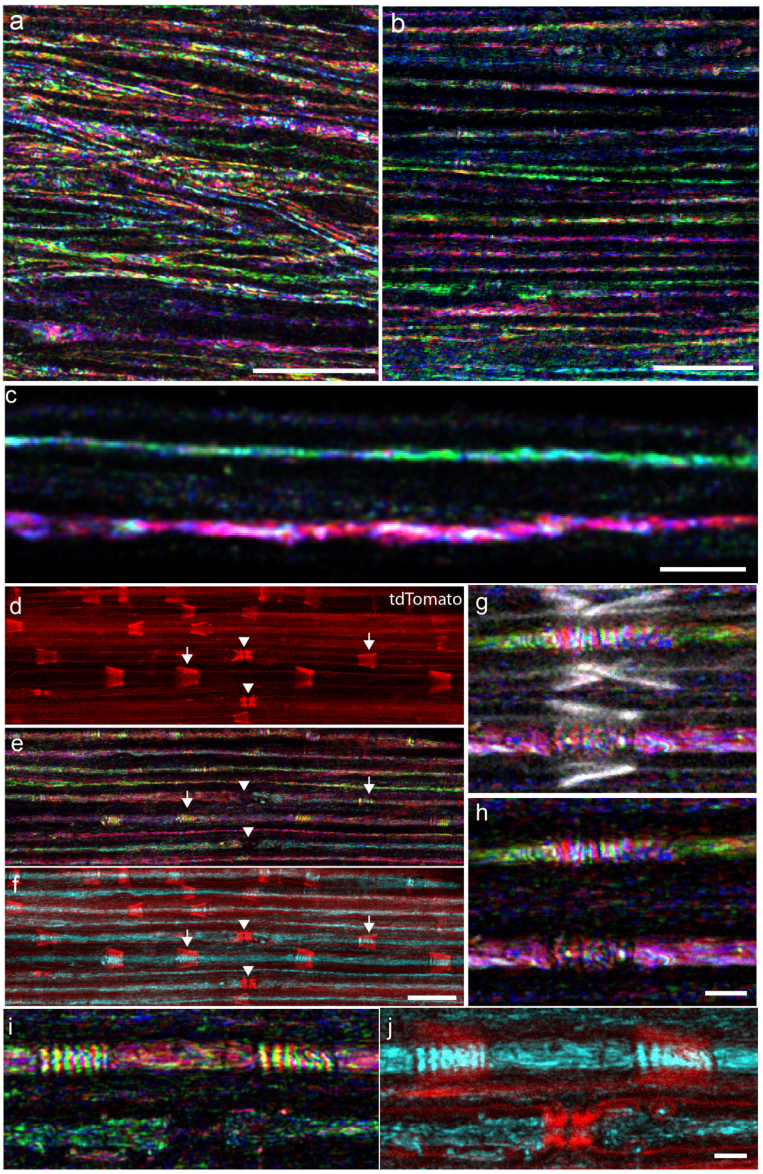

Figure 4. Multicolor reflection spectrum reveals distinct myelin structures in the spinal cord and sciatic nerve *in vivo*

(**a–b**) Multicolor SCoRe images captured from the spinal cord (**a**) and sciatic nerve (**b**) showing that individual fibers reflect different colors but have a predominant color consistency along each axon. 25 μm scale bars. (**c**) Two differentially reflecting axons in the sciatic nerve at high-resolution. 10 μm scale bar. (**d–f**) *In vivo* SCoRe and fluorescence images captured from an mT/mG mouse expressing tdTomato in myelin sheaths (red) (**d**) showing Schmidt-Lanterman incisures (arrows) and nodes of Ranvier (arrowheads) (**e**). Combined reflection image in cyan is shown in composite with tdTomato in (**f**). 20 μm scale bar in d–f. (**g–h**) High magnification image of two Schmidt-Lanterman incisures showing SCoRe vertical interference pattern and fluorescent tdTomato (white) overlay (**g**) and SCoRe alone (**h**). (**i–j**) High magnification images of two Schmidt-Lanterman incisures and one node of Ranvier showing all reflected lasers (**i**) and combined reflection (cyan) with

tdTomato fluorescence (red) (**j**). 4 μm scale bar in g–j (experiments were replicated 3 times in n= 8 mice for spinal cord, n=10 mice for sciatic nerve).

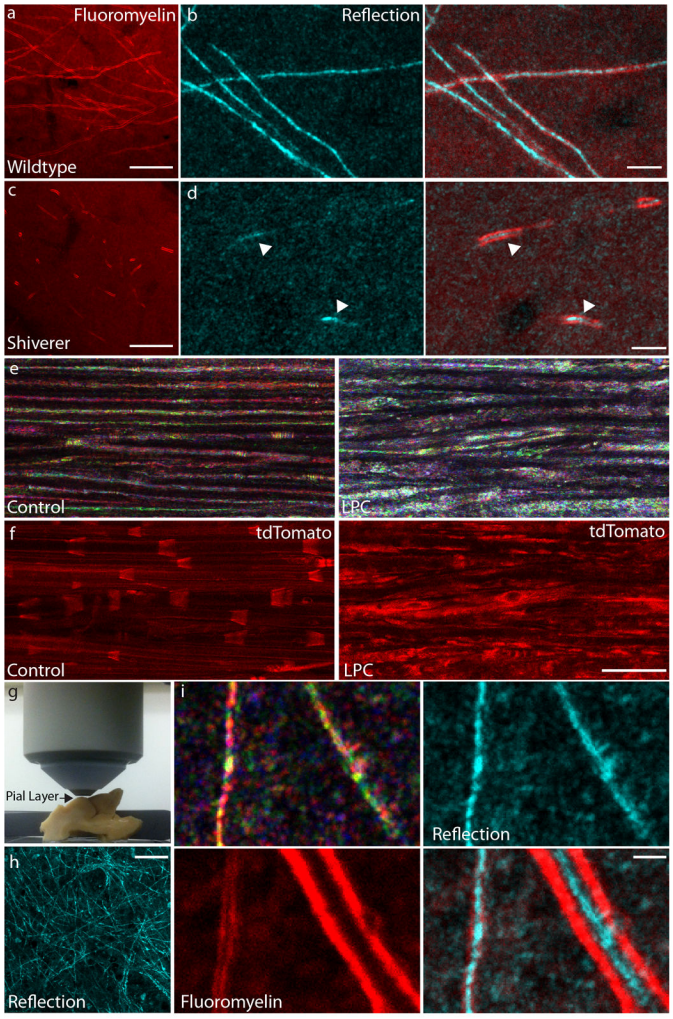

Figure 5. Myelin pathology and human myelinated axons imaged with SCoRe

(**a–d**) Images captured through a cranial window in P35 wildtype (n=3 mice, 5 replicates) (**a–b**) and congenitally hypomyelinated *shiverer* mouse (n=2 mice, 4 replicates) (**c–d**). In *shiverer*, we saw small patches of Fluoromyelin (FM)-labeled myelinated axon segments (**c**), which we never observed in wildtype mice (**a**). These patches were also reflective only in the region that was FM-labeled (**d,** arrowheads). 25 μm scale bar in **a**,**c**, 5 μm in **b,d**. (**e–f**) Images acquired *in vivo* from the sciatic nerve of an mT/mG mouse with membrane bound tdTomato before (left) and after (right) intraneural injection of the demyelinating agent lysophosphatidylcholine (LPC), showing an acute change in the reflected spectrum (**e**) and in the tdTomato fluorescence distribution (**f**). 30 μm scale bar in **e–f** (n=3 mice, 3 replicates). (**g**) Photograph showing the setup for SCoRe imaging of the cortex through the pial surface in a fixed human brain explant. (**h**) Z-projection reflection image obtained from the human brain explant. 30 μm scale bar. (**i**) High-magnification multicolor (top left) and combined (cyan) images of two myelinated reflective fibers demonstrated by Fluoromyelin labeling (red). 3 μm scale bar.